

# On the Feynman-Hellmann Theorem in Quantum Field Theory and the Calculation of Matrix Elements

Chris Bouchard,<sup>1,2,\*</sup> Chia Cheng Chang (張家丞),<sup>3,†</sup>  
Thorsten Kurth,<sup>3,4,‡</sup> Kostas Orginos,<sup>2,5,§</sup> and André Walker-Loud<sup>3,2,5,¶</sup>

<sup>1</sup>*School of Physics and Astronomy, University of Glasgow, Glasgow G12 8QQ, UK*

<sup>2</sup>*Department of Physics, The College of William & Mary Williamsburg, VA 23187-8795, USA*

<sup>3</sup>*Nuclear Science Division, Lawrence Berkeley National Laboratory, Berkeley, CA 94720, USA*

<sup>4</sup>*NERSC, Lawrence Berkeley National Laboratory, Berkeley, CA 94720, USA*

<sup>5</sup>*Thomas Jefferson National Accelerator Facility Newport News, VA 23606, USA*

The Feynman-Hellmann Theorem can be derived from the long Euclidean-time limit of correlation functions determined with functional derivatives of the partition function. Using this insight, we develop an improved method for computing matrix elements of external currents utilizing only two-point correlation functions. Our method applies to matrix elements of any external bi-linear current, including non-zero momentum transfer, flavor-changing, and two-current insertion matrix elements. The contamination from excited states is shown to be Euclidean-time dependent allowing for a significantly improved ability to reliably determine and control the systematics. We demonstrate the utility of our method with a calculation of the nucleon axial-charge using gradient-flowed domain-wall valence quarks on the  $N_f = 2 + 1 + 1$  MILC highly-improved staggered quark (HISQ) ensemble with lattice spacing and pion mass of approximately 0.15 fm and 310 MeV respectively. We show full control over excited state systematics with the new method and obtain value of  $g_A = 1.213(26)$  with a quark-mass dependent renormalization coefficient.

## I. INTRODUCTION

The Feynman-Hellmann Theorem (FHT) in quantum mechanics relates matrix elements to variations in the spectrum [1–4]:

$$\frac{\partial E_n}{\partial \lambda} = \langle n | H_\lambda | n \rangle, \quad (1)$$

where the Hamiltonian is given by  $H = H_0 + \lambda H_\lambda$ . This simple relation follows straightforwardly at first order in perturbation theory. The method is applicable beyond perturbation theory and is often used in lattice QCD (LQCD) calculations, for example, to compute the scalar quark matrix elements in the nucleon [5–20]

$$m_q \frac{\partial m_N}{\partial m_q} \Big|_{m_q=m_q^{\text{phys}}} = \langle N | m_q \bar{q}q | N \rangle, \quad (2)$$

for the light ( $q = \{u, d\}$ ) and strange ( $q = s$ ) quarks. Quantitative knowledge of these matrix elements is necessary for interpreting direct searches for dark matter which look for the elastic recoil of nuclei. In the scenario that dark matter is heavy and couples through the electroweak sector, the uncertainty on the strange and charm nucleon matrix elements is one of the largest uncertainties in spin-independent constraints upon direct dark matter detection [21]. In particular, due to cancellations in the amplitude at the level of quarks and gluons,

there is a particular sensitivity to the scalar charm quark matrix elements with current uncertainties allowing for several orders of magnitude variability in the cross section, see Fig. 3 of Ref. [21]. A significant reduction over the current uncertainty in these matrix elements would be a welcome advancement for the field.

Recently, the FHT has been used to compute other nucleon matrix elements, such as the spin content of the nucleon [22, 23]. More recently, a hybrid method using ideas from background field methods [24–30] and the FHT has been introduced to compute few-nucleon electroweak matrix elements [31]. An advantage of the FHT is that it relates a three-point correlation function to a change in a two-point correlation function induced by an external source. Thus, one can take advantage of the simplified analyses of two-point functions. Traditional lattice calculations of three-point functions, particularly those involving nucleons, face a number of challenging systematics beyond those present for two-point functions: the stochastic noise of three-point functions is more severe than the corresponding two-point functions and also three-point functions have systematic contamination from excited states which is constant in Euclidean time for fixed source-sink separation. Controlling these systematics requires a significant increase in the numerical cost.

Previous implementations of the FHT and related methods [22, 23, 31] are also costly, as the calculation must be performed for several values of the external parameter,  $\lambda$ . In the case of the scalar quark matrix elements, the QCD action contains the operators of interest,  $\lambda = m_q$ . The FHT is then simply used by varying the values of the quark masses and determining the resulting variation of the spectrum, a routine step in present LQCD calculations. In the case of the nucleon spin, the

\* [chris.bouchard@glasgow.ac.uk](mailto:chris.bouchard@glasgow.ac.uk)

† [chiachang@lbl.gov](mailto:chiachang@lbl.gov)

‡ [tkurth@lbl.gov](mailto:tkurth@lbl.gov)

§ [kostas@wm.edu](mailto:kostas@wm.edu)

¶ [awalker-loud@lbl.gov](mailto:awalker-loud@lbl.gov)

operator  $\lambda \bar{q} \gamma_\mu \gamma_5 q$  is perturbatively added to the theory for varying values of  $\lambda$  and the resulting spectrum is computed such that  $\partial_\lambda E_n(\lambda)$  can be approximated via finite difference.

In this work, we develop an improved implementation of the FHT and explore its connection with the partition function of quantum field theory. This new method offers several advantages including: an improved implementation, increased stochastic sampling over computations of equal computing time, a complete discussion of all systematics, and demonstrably rigorous control over all systematics associated with analysis of correlation functions. To demonstrate these claims, we present the formulation of our method, and perform a sample calculation of the nucleon axial-vector charge. We then discuss the generalizations and conclude.

## II. THE FEYNMAN-HELLMANN THEOREM AND A NEW METHOD

### A. The New Method

Consider a two point correlation function computed in the presence of some external source

$$\begin{aligned} C_\lambda(t) &= \langle \lambda | \mathcal{O}(t) \mathcal{O}^\dagger(0) | \lambda \rangle \\ &= \frac{1}{\mathcal{Z}_\lambda} \int D\Phi e^{-S - S_\lambda} \mathcal{O}(t) \mathcal{O}^\dagger(0) \end{aligned} \quad (3)$$

with the external source coupled through some bi-linear current density  $j(x)$

$$S_\lambda = \lambda \int d^4x j(x), \quad (4)$$

and partition function in the presence of the source,

$$\mathcal{Z}_\lambda = \int D\Phi e^{-S - S_\lambda}. \quad (5)$$

Here,  $\Phi$  is a general field operator representing the various quantum fields of the theory. The state  $|\lambda\rangle$  is the vacuum state in the presence of the external source. We denote the source-less vacuum state, partition function, and two point correlation function by

$$|\Omega\rangle = \lim_{\lambda \rightarrow 0} |\lambda\rangle, \quad (6)$$

$$\mathcal{Z} = \lim_{\lambda \rightarrow 0} \mathcal{Z}_\lambda, \quad (7)$$

$$C(t) = \lim_{\lambda \rightarrow 0} C_\lambda(t), \quad (8)$$

respectively. The operator  $\mathcal{O}^\dagger(0)$  creates a tower of states with specified quantum numbers out of the vacuum at time  $t = 0$ , which are later destroyed by a conjugate operator  $\mathcal{O}(t)$  at time  $t$ .

We are interested in the partial derivative of this correlation function with respect to  $\lambda$ , at  $\lambda = 0$ . This partial

derivative can be built from an integral of uniform functional derivatives over the space-time volume. Or, if we wish for more general matrix elements, such as those involving momentum transfer, an integral over non-uniform values of  $\lambda(x)$ . For now, we will focus on the simplest case of a constant source,  $\lambda(x) = \lambda$ .

The partial derivative of interest is related to the matrix elements of the current  $j(x)$

$$\begin{aligned} - \frac{\partial C_\lambda(t)}{\partial \lambda} \Big|_{\lambda=0} &= \frac{\partial \mathcal{Z}_\lambda}{\partial \lambda} \Big|_{\lambda=0} \frac{C(t)}{\mathcal{Z}} \\ &+ \frac{1}{\mathcal{Z}} \int D\Phi e^{-S} \int d^4x' j(x') \mathcal{O}(t) \mathcal{O}^\dagger(0). \end{aligned} \quad (9)$$

The first term is proportional to the vacuum matrix element of the current and vanishes unless the current has vacuum quantum numbers. The second term involves an integral over matrix elements involving the current and the creation/annihilation operators:

$$\begin{aligned} - \frac{\partial C_\lambda(t)}{\partial \lambda} \Big|_{\lambda=0} &= -C(t) \int dt' \langle \Omega | J(t') | \Omega \rangle \\ &+ \int dt' \langle \Omega | T \{ \mathcal{O}(t) J(t') \mathcal{O}^\dagger(0) \} | \Omega \rangle \end{aligned} \quad (10)$$

where we have defined  $J(t) = \int d^3x j(t, \vec{x})$ . The second term is related to the hadronic matrix of interest in the time region  $0 < t' < t$ . In the other time regions,  $t' < 0$  and  $t' > t$ , the current  $J$  creates/destroys a tower of states that also couple to the states created by  $\mathcal{O}$  (in the case of quark bi-linear operators in QCD, these are just the mesons coupled to the  $\bar{q} \Gamma q$  currents):

$$\begin{aligned} \int dt' \langle \Omega | T \{ \mathcal{O}(t) J(t') \mathcal{O}^\dagger(0) \} | \Omega \rangle &= \\ &\int_{-\infty}^0 dt' \langle \Omega | \mathcal{O}(t) \mathcal{O}^\dagger(0) J(t') | \Omega \rangle \\ &+ \int_0^t dt' \langle \Omega | \mathcal{O}(t) J(t') \mathcal{O}^\dagger(0) | \Omega \rangle \\ &+ \int_t^\infty dt' \langle \Omega | J(t') \mathcal{O}(t) \mathcal{O}^\dagger(0) | \Omega \rangle. \end{aligned} \quad (11)$$

Recall, the FHT relates matrix elements to derivatives of the spectrum. In Euclidean calculations, the effective mass is a derived quantity which asymptotes to the ground state energy in the long time limit,

$$m^{\text{eff}}(t, \tau) = \frac{1}{\tau} \ln \left( \frac{C(t)}{C(t+\tau)} \right) \xrightarrow{t \rightarrow \infty} \frac{1}{\tau} \ln(e^{E_0 \tau}). \quad (12)$$

In analogy with the FHT, consider the linear response of the effective mass to the external current

$$\frac{\partial m_\lambda^{\text{eff}}(t, \tau)}{\partial \lambda} \Big|_{\lambda=0} = \frac{1}{\tau} \left[ \frac{\partial_\lambda C_\lambda(t+\tau)}{C(t+\tau)} - \frac{\partial_\lambda C_\lambda(t)}{C(t)} \right] \Big|_{\lambda=0}. \quad (13)$$

A first observation to make is that the term proportional to the vacuum matrix element in Eq. (10) exactly

cancels in the difference in Eq. (13). The linear response of the effective mass is therefore given by

$$\left. \frac{\partial m_\lambda^{\text{eff}}(t, \tau)}{\partial \lambda} \right|_{\lambda=0} = \frac{R(t+\tau) - R(t)}{\tau} \quad (14)$$

where

$$R(t) \equiv \frac{\int dt' \langle \Omega | T \{ \mathcal{O}(t) J(t') \mathcal{O}^\dagger(0) \} | \Omega \rangle}{C(t)}. \quad (15)$$

This expression can be analyzed with the usual spectral decomposition. The two-point correlation function in time-momentum space, with  $\mathbf{p} = \mathbf{0}$ , is given by

$$\begin{aligned} C(t, \mathbf{0}) &= \sum_{\mathbf{x}} \langle \Omega | \mathcal{O}(t, \mathbf{x}) \mathcal{O}^\dagger(0, \mathbf{0}) | \Omega \rangle \\ &= \sum_n \frac{Z_n^0 Z_n^\dagger}{2E_n} e^{-E_n t} \end{aligned} \quad (16)$$

which can be obtained by inserting the identity operator

$$1 = |\Omega\rangle\langle\Omega| + \sum_n \int \frac{d^3 p}{2E_n(p)} |n, \mathbf{p}\rangle\langle n, \mathbf{p}|. \quad (17)$$

The overlap factors are defined as

$$\begin{aligned} Z_n^\dagger &= \langle n | \mathcal{O}^\dagger(0, \mathbf{0}) | \Omega \rangle, \\ Z_n^{\mathbf{p}} &= \sum_{\mathbf{x}} e^{i\mathbf{p}\cdot\mathbf{x}} \langle \Omega | \mathcal{O}(0, \mathbf{x}) | n \rangle. \end{aligned} \quad (18)$$

The numerator in Eq. (15) can be similarly decomposed. It is useful to work in discrete Euclidean time relevant to LQCD calculations in which the numerator is

$$N(t) = \sum_{t'=0}^{T-1} \langle 0 | T \{ \mathcal{O}(t) J(t') \mathcal{O}^\dagger(0) \} | 0 \rangle. \quad (19)$$

There are 4 time regions to consider, depicted in Figure 1:

$$\begin{aligned} \text{I: } 0 < t' < t, & & \text{II: } t < t' < T-1, \\ \text{III: } t' = 0, & & \text{IV: } t' = t. \end{aligned} \quad (20)$$

The matrix elements of interest occur in time-region I, when the current is inserted between the source/sink creation/annihilation interpolating fields. The contributions from regions II, III and IV are systematic corrections which must be accounted for and controlled. In region II, the current creates/destroys a meson with the quantum numbers of the current outside the region of interest. Regions III and IV give rise to *contact operators* when the current insertion time occurs precisely at the creation or annihilation time of the hadron.

In the first region,  $0 < t' < t$ , the numerator is

$$N_{\text{I}}(t) = \sum_{t'=1}^{t-1} \sum_{\beta} \frac{e^{-E_\beta T}}{\mathcal{N}_\beta} \langle \beta | \mathcal{O}(t) J(t') \mathcal{O}^\dagger(0) | \beta \rangle, \quad (21)$$

where  $\mathcal{N}_\beta = 1$  for the vacuum and  $\mathcal{N}_\beta = 2E_\beta$  otherwise. All thermal states will be exponentially suppressed and we can consider the contribution from just the vacuum state  $|\beta\rangle = |\Omega\rangle$ . In this case, we have

$$\begin{aligned} N_{\text{I}}(t) &= \sum_{t'=1}^{t-1} \sum_{n,m} \langle \Omega | \mathcal{O}(t) \frac{|n\rangle\langle n|}{2E_n} J(t') \frac{|m\rangle\langle m|}{2E_m} \mathcal{O}^\dagger(0) | \Omega \rangle \\ &= \sum_{t'=1}^{t-1} \sum_{n,m} \frac{Z_n^0 Z_m^\dagger}{4E_n E_m} \langle n | J | m \rangle e^{-E_n t} e^{-(E_m - E_n)t'} \\ &= \sum_{t'=1}^{t-1} \left[ \sum_n \frac{Z_n^0 Z_n^\dagger}{4E_n^2} \langle n | J | n \rangle e^{-E_n t} \right. \\ &\quad \left. + \sum_{n \neq m} \frac{Z_n^0 Z_m^\dagger}{4E_n E_m} \langle n | J | m \rangle e^{-E_n t} e^{-(E_m - E_n)t'} \right]. \end{aligned} \quad (22)$$

The first term is independent of  $t'$  and is thus enhanced by an overall factor of  $t-1$ . The  $t'$  dependence of the second term is contained entirely in the exponential factor

$$\sum_{t'=1}^{t-1} e^{-(E_m - E_n)t'} = \frac{1 - e^{-\Delta_{mn}(t-1)}}{e^{\Delta_{mn}} - 1}, \quad (23)$$

where we have defined

$$\Delta_{mn} \equiv E_m - E_n. \quad (24)$$

The contributions from region I are then

$$\begin{aligned} N_{\text{I}}(t) &= (t-1) \sum_n \frac{Z_n^0 Z_n^\dagger}{4E_n^2} e^{-E_n t} J_{nn} \\ &+ \sum_{n,m \neq n} \frac{Z_n^0 Z_m^\dagger}{4E_n E_m} \frac{e^{-E_n t - \frac{\Delta_{mn}}{2}} - e^{-E_m t - \frac{\Delta_{nm}}{2}}}{e^{\frac{\Delta_{mn}}{2}} - e^{\frac{\Delta_{nm}}{2}}} J_{nm}, \end{aligned} \quad (25)$$

where we have defined  $J_{nm} \equiv \langle n | J | m \rangle$  and written the expression to expose the  $n \leftrightarrow m$  symmetry. The only terms which do not also appear in the two point correlation functions are the matrix elements of interest,  $J_{nm}$ . It is worth noting the entire contribution from region I vanishes at  $t = 1$ .

Let us now consider the contribution from region II,

$$N_{\text{II}}(t) = \sum_{t'=t+1}^{T-1} \sum_{\beta} \frac{e^{-E_\beta T}}{\mathcal{N}_\beta} \langle \beta | J(t') \mathcal{O}(t) \mathcal{O}^\dagger(0) | \beta \rangle. \quad (26)$$

To understand the systematics from this region, we can not immediately drop the non-vacuum contributions from the thermal sum. Inserting a complete set of states,

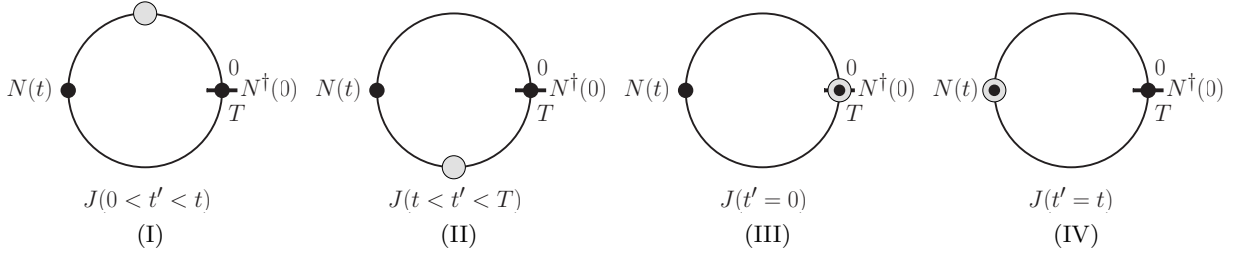


FIG. 1. The 4 different current insertion time regions. The matrix element of interest occurs in region I:  $0 < t' < t$ . Regions II, III and IV are systematic corrections which must be accounted for where III and IV arise from contact operators. The horizontal black line represents the temporal boundary with (anti)periodic boundary conditions. The solid black circles represent the hadron creation/annihilation operators and the light grey circle is the current insertion.

one finds

$$\begin{aligned}
N_{\text{II}}(t) &= \sum_{\beta, \alpha, n} J_{\beta\alpha} \langle \alpha | \mathcal{O} | n \rangle \langle n | \mathcal{O}^\dagger | \beta \rangle \frac{e^{-E_\beta T} e^{E_\alpha t} e^{-E_n t}}{\mathcal{N}_\alpha \mathcal{N}_\beta \mathcal{N}_n} \\
&\times \sum_{t'=t+1}^{T-1} e^{t' \Delta_{\beta\alpha}} \\
&= \sum_{\beta, \alpha, n} \frac{J_{\beta\alpha} \langle \alpha | \mathcal{O} | n \rangle \langle n | \mathcal{O}^\dagger | \beta \rangle}{\mathcal{N}_\alpha \mathcal{N}_\beta \mathcal{N}_n} e^{-E_n t} \\
&\times \frac{e^{-E_\alpha(T-t)} e^{\Delta_{\alpha\beta}/2} - e^{-E_\beta(T-t)} e^{\Delta_{\beta\alpha}/2}}{e^{\Delta_{\beta\alpha}/2} - e^{\Delta_{\alpha\beta}/2}}. \quad (27)
\end{aligned}$$

For small  $t$ , we can neglect all but the vacuum contribution in the sum over  $\alpha$  and  $\beta$  for the first and second terms respectively. The region II contributions are then

$$\begin{aligned}
N_{\text{II}}(t) &= \sum_n \frac{e^{-E_n t}}{2E_n} \left\{ Z_n^0 Z_n^\dagger \langle \Omega | J | \Omega \rangle \right. \\
&\quad \left. + \sum_j \frac{Z_n^0 Z_{nj}^\dagger J_j^\dagger + J_j Z_{jn}^0 Z_n^\dagger}{2E_j (e^{E_j} - 1)} \right\} \quad (28)
\end{aligned}$$

where we have defined

$$J_j^\dagger \equiv \langle j | J | \Omega \rangle, \quad Z_{nj}^\dagger \equiv \langle n | \mathcal{O}^\dagger | j \rangle. \quad (29)$$

Note the first term in Eq. (28) only contributes for scalar currents.

Finally, there is the contribution from the contact terms, regions III and IV, when  $t' = 0$  or  $t' = t$ . These contact contributions are standard two-point functions with different interpolating operators

$$N_{\text{III}}(t) = \sum_{\beta, n} \frac{e^{-E_\beta T}}{\mathcal{N}_\beta} \langle \beta | \mathcal{O}(t) \frac{|n\rangle\langle n|}{2E_n} J(0) \mathcal{O}^\dagger(0) | \beta \rangle, \quad (30)$$

$$N_{\text{IV}}(t) = \sum_{\beta, n} \frac{e^{-E_\beta T}}{\mathcal{N}_\beta} \langle \beta | \mathcal{O}(t) J(t) \frac{|n\rangle\langle n|}{2E_n} \mathcal{O}^\dagger(0) | \beta \rangle. \quad (31)$$

In both terms, the thermal contributions are suppressed for all but the vacuum contribution. These two terms

then contribute

$$N_{\text{III+IV}}(t) = \sum_n \frac{e^{-E_n t}}{2E_n} \left[ Z_n^0 Z_{J:n}^\dagger + Z_{J:n}^0 Z_n^\dagger \right], \quad (32)$$

where we have defined

$$Z_{J:n}^\dagger \equiv \langle n | J \mathcal{O}^\dagger | \Omega \rangle. \quad (33)$$

Because the states  $|n\rangle$  are annihilated by the same operator as in the two-point function, the sum over states in Eq. (32) is over the same set of states as the two-point function but with modified overlap factors.

Putting all the regions together, the numerator is

$$\begin{aligned}
N(t) &= \sum_n \left\{ \frac{e^{-E_n t}}{2E_n} \left[ (t-1) J_{nm} \frac{Z_n^0 Z_n^\dagger}{2E_n} \right. \right. \\
&\quad \left. \left. + Z_n^0 Z_{J:n}^\dagger + Z_{J:n}^0 Z_n^\dagger + Z_n^0 Z_n^\dagger \langle \Omega | J | \Omega \rangle \right] \right. \\
&\quad \left. + \sum_j \frac{Z_n^0 Z_{nj}^\dagger J_j^\dagger + J_j Z_{jn}^0 Z_n^\dagger}{2E_j (e^{E_j} - 1)} \right] \\
&\quad \left. + \sum_{m \neq n} \frac{Z_n^0 Z_m^\dagger}{4E_n E_m} \frac{e^{-E_n t - \frac{\Delta_{mn}}{2}} - e^{-E_m t - \frac{\Delta_{nm}}{2}}}{e^{\frac{\Delta_{mn}}{2}} - e^{\frac{\Delta_{nm}}{2}}} J_{nm} \right\}. \quad (34)
\end{aligned}$$

The simplicity of our method is recovered by substituting Eqs. (16) and (34) into Eq. (13), where in the long-time limit, we obtain directly the expression for the ground state matrix element of interest,

$$\lim_{t \rightarrow \infty} \frac{\partial m_\lambda^{\text{eff}}(t, \tau)}{\partial \lambda} \Big|_{\lambda=0} = \frac{J_{00}}{2E_0}. \quad (35)$$

## B. Implementation

The numerical implementation of this new method is straightforward. What is needed is the construction of the derivative correlation function, Eq. (11). We provide an explicit example of a non-scalar current  $J_\Gamma$  with interpolating operators coupling to the proton. Standard

proton creation and annihilation operators are given by

$$\begin{aligned}\bar{N}_{\gamma'}(x) &= \epsilon_{i'j'k'} \left( \bar{u}_{\alpha'}^{i'}(x) \Gamma_{\alpha'\beta'}^{src} \bar{d}_{\beta'}^{j'}(x) \right) P_{\gamma'\rho'}^{src} \bar{u}_{\rho'}^{k'}(x), \\ N_{\gamma}(y) &= -\epsilon_{ijk} \left( u_{\alpha}^i(y) \Gamma_{\alpha\beta}^{snk} d_{\beta}^j(y) \right) P_{\gamma\rho}^{snk} u_{\rho}^k(y),\end{aligned}\quad (36)$$

where  $u(x)$  and  $d(x)$  are up and down quark field operators at  $x$ . The  $\Gamma^{src}$ ,  $\Gamma^{snk}$ ,  $P^{src}$  and  $P^{snk}$  are spin projectors used to project onto the total spin of the proton. For example, working in the Dirac basis, the dominant spin-up local interpolating field can be constructed using [32, 33] (where the spinor indices are labeled 1,2,3,4)

$$P^{src} = \delta_{\mu,1}, \quad \Gamma^{src} = \begin{pmatrix} 0 & 1 & 0 & 0 \\ -1 & 0 & 0 & 0 \\ 0 & 0 & 0 & 0 \\ 0 & 0 & 0 & 0 \end{pmatrix}, \quad (37)$$

and similar operators for the sink. Denoting the up and down quark propagators as

$$\begin{aligned}U(y, x)_{\alpha\alpha'}^{ii'} &= \underline{u}_{\alpha}^i(y) \bar{u}_{\alpha'}^{i'}(x), \\ D(y, x)_{\alpha\alpha'}^{ii'} &= \underline{d}_{\alpha}^i(y) \bar{d}_{\alpha'}^{i'}(x),\end{aligned}\quad (38)$$

the proton correlation function is given by

$$\begin{aligned}C_{\gamma\gamma'} &= \epsilon_{ijk} P_{\gamma\rho}^{snk} \left[ (\Gamma^{snk} D)_{\alpha\beta'}^{ii'} (U \Gamma^{src})_{\alpha\beta'}^{jj'} U_{\rho\rho'}^{kk'} \right. \\ &\quad \left. + (U \Gamma^{src})_{\rho\beta'}^{kk'} U_{\alpha\rho'}^{ii'} (\Gamma^{snk} D)_{\alpha\beta'}^{jj'} \right] P_{\gamma'\rho'}^{src} \epsilon_{i'j'k'}.\end{aligned}\quad (39)$$

The derivative correlation function  $(-\partial_{\lambda} C|_{\lambda=0})$  is trivially determined. Applying the partial derivative in Eq. (10) at the level of the path integral, one immediately observes the derivative correlation function is obtained with the replacement of one of the quark propagators in the two-point correlation function with a *Feynman-Hellmann* (FH) propagator, summed over all possible insertions, where the FH propagator is simply a sequential propagator which is also summed over the current insertion time

$$S^{\Gamma}(y, x) = \sum_{z=(t_z, \mathbf{z})} S(y, z) \Gamma S(z, x). \quad (40)$$

This extra sum leads to an  $\mathcal{O}(T)$  stochastic enhancement of the resulting derivative correlation function as compared to the standard method with a sequential propagator. The idea of using this propagator in a two-point function can be traced back to Ref. [34], where the equivalent of Eq. (15) is approximated with its long-time limit and computed for various hadronic matrix elements. This idea has been extended recently in Refs. [35, 36] with an application to derivatives with respect to  $Q^2$  of mesonic structure functions in Ref. [35].

For our present example, the proton derivative correlation function with a current insertion on the down-quark is given by  $D \rightarrow D^{\Gamma}$

$$\begin{aligned}C_{\gamma\gamma'}^{\Gamma_d} &= \epsilon_{ijk} P_{\gamma\rho}^{snk} \left[ (\Gamma^{snk} D^{\Gamma})_{\alpha\beta'}^{ii'} (U \Gamma^{src})_{\alpha\beta'}^{jj'} U_{\rho\rho'}^{kk'} \right. \\ &\quad \left. + (U \Gamma^{src})_{\rho\beta'}^{kk'} U_{\alpha\rho'}^{ii'} (\Gamma^{snk} D^{\Gamma})_{\alpha\beta'}^{jj'} \right] P_{\gamma'\rho'}^{src} \epsilon_{i'j'k'},\end{aligned}\quad (41)$$

while for a current insertion on the up-quark, one has

$$\begin{aligned}C_{\gamma\gamma'}^{\Gamma_u} &= \epsilon_{ijk} P_{\gamma\rho}^{snk} \left[ (\Gamma^{snk} D)_{\alpha\beta'}^{ii'} (U \Gamma^{src})_{\alpha\beta'}^{jj'} U_{\rho\rho'}^{kk'} \right. \\ &\quad \left. + (\Gamma^{snk} D)_{\alpha\beta'}^{ii'} (U \Gamma^{src})_{\alpha\beta'}^{jj'} U_{\rho\rho'}^{\Gamma, kk'} \right. \\ &\quad \left. + (U \Gamma^{src})_{\rho\beta'}^{kk'} U_{\alpha\rho'}^{ii'} (\Gamma^{snk} D)_{\alpha\beta'}^{jj'} \right. \\ &\quad \left. + (U \Gamma^{src})_{\rho\beta'}^{kk'} U_{\alpha\rho'}^{\Gamma, ii'} (\Gamma^{snk} D)_{\alpha\beta'}^{jj'} \right] P_{\gamma'\rho'}^{src} \epsilon_{i'j'k'}.\end{aligned}\quad (42)$$

These correlators are functions of the source-sink separation time in contrast to the fixed source-sink separation time dependence of the standard three-point correlators constructed with sequential propagators. It is trivial to generalize this construction to an arbitrary correlation function with the successive replacement of each quark propagator with its respective FH propagator.

For scalar current matrix elements, one must also consider contributions from disconnected diagrams. While disconnected diagrams are stochastically noisier, we may be able to improve upon the general method as we have the freedom to compute the disconnected quark loop as a function of Euclidean time. Instead of summing over all time as in Eq. (11), we can explicitly choose to only sum over the time window  $0 < t' < t$ , thus including only the contributions of interest, Eq. (25). It is worth exploring if this suggestion provides an improved determination of the disconnected contributions.

### III. AN APPLICATION TO THE NUCLEON AXIAL CHARGE

We demonstrate the use of this method by computing the nucleon isovector axial charge on one of the publicly available 2+1+1 HISQ [37] ensembles from the MILC Collaboration [38], with  $a \simeq 0.15$  fm,  $m_{\pi} \simeq 310$  MeV and a lattice volume of  $16^3 \times 48$ . The present work utilizes 1960 configurations with 6 sources per configuration. The HISQ configurations are first gradient-flowed to smear out the UV fluctuations. Möbius Domain-Wall fermion (MDWF) [39] propagators are then solved with the QUDA library [40] with multi-GPU support [41]. The valence quark mass is tuned such that the MDWF pion mass matches the taste-5 HISQ pion mass within 1%. We then construct the isovector nucleon two-point and derivative FH correlation functions. We further double our statistics by including the time-reversed correlation functions constructed with negative parity nucleon operators. The calculation requires solving both the regular and the FH propagator for each source. The motivation and advantages of such a mixed-action are described in Ref. [42]. This action has also been used to compute the  $\pi^{-} \rightarrow \pi^{+}$  matrix element relevant to  $0\nu\beta\beta$  (neutrinoless double beta-decay) [43].

### A. Fit strategy

We extract the isovector nucleon charge by applying two analysis strategies: we apply a standard Frequentist analysis of our results as well as a Bayesian constrained fit with Gaussian priors on the two- and three-point correlation functions following the framework of Ref. [44]. While we find consistent answers with both analysis strategies, the Bayesian analysis allows us to more rigorously and completely explore the fitting systematics, thus demonstrating the efficacy of this new method. Controlling fitting systematics for nucleons is critical for current and future LQCD calculations. Similar ideas of Bayesian constrained curve fits were explored in Ref. [45] and recently used in Ref. [46].

In our present Bayesian analysis, we observe stability in all ground state parameters under variations of the number of time slices in our data, and number of states in our fit ansatz, demonstrating complete control over systematic uncertainty originating from the fitting procedure. We rate the quality of our fits by the  $Q$ -statistic, which is related to the Frequentist  $p$ -value as defined in Eq. (B4) of Ref. [47] and consider only fits with  $Q > 0.1$ . We select results from different fit ansatzes by comparing Bayes Factors, and make distinctions between models if the Bayes Factor is larger than 3. Constrained curve fits are implemented by the software package `lsqfit` [48].

In the following sections, the fit procedure is first discussed for the two-point correlation function. The preferred two-point fit is then performed simultaneously with the three-point correlator leading to our final value for  $g_A$ . We adopt the notation of placing a tilde on top of the parameter (*e.g.*  $E_0$ ) to denote its prior distribution (*e.g.*  $\tilde{E}_0$ ), and a hat (*e.g.*  $\hat{E}_0$ ) to denote its posterior distribution.

### B. Two-point correlator analysis

#### 1. Fit strategy

The two-point fit ansatz is given by Eq. (16) and has a sum over the infinite tower of states. Without loss of generality, we redefine the overlap factors as  $z_n \equiv Z_n/\sqrt{2E_n}$  and employ the following two-point fit ansatz for the rest of the analysis,

$$C(t, \mathbf{0}) = \sum_n z_n^0 z_n^\dagger e^{-E_n t}. \quad (43)$$

We focus on the case of zero momentum insertion and drop the superscript momentum label,  $z_n^0 \rightarrow z_n$ . In the following section, we detail how the priors are set for the infinite number of states, and quantitatively show where the series may be truncated.

We begin our two-point analysis by looking at the effective mass as defined in Eq. (12) and shown in Figs. 2 and 3. We observe a plateau indicating that the ground

state energy has a value of approximately  $E_0 \approx 0.82$ . We set a loose prior of  $\tilde{E}_0 = 0.82(4)$  as indicated by the light blue band. The width of the prior is observed to be approximately one order of magnitude larger than the resulting posterior distribution, which is indicated by the dark blue band.

Using the estimate of  $E_0$ , we construct the scaled two-point function in order to set prior distributions for  $\tilde{z}_0^S$  and  $\tilde{z}_0^P$ , which are respectively the ground state smeared and point overlap-factors. We define the scaled correlators as

$$z_S^{\text{eff}}(t) = \sqrt{C_{SS}(t)} e^{\tilde{E}_0 t}, \quad (44)$$

$$z_P^{\text{eff}}(t) = C_{PS}(t) e^{\tilde{E}_0 t} / z_S^{\text{eff}}(t), \quad (45)$$

where  $C_{SS}(t)$  and  $C_{PS}(t)$  are the smeared-smeared and point-smeared two-point functions, respectively. From the redefinition of Eq. (43), the scaled correlators plateau to  $z_0^{S(P)}$  in the  $t \rightarrow \infty$  limit. From Fig. 4, we assign approximate values for the overlap factors, and set prior widths to half the magnitude of the expected central value leading to  $\tilde{z}_0^S = 0.0004(2)$  and  $\tilde{z}_0^P = 0.010(5)$ . These priors are unconstraining since the widths of the posterior distributions are approximately two orders of magnitude smaller.

We introduce priors for the excited state energies as energy splittings, enforcing a hierarchy of states. This is achieved by setting the energy splitting with a lognormal prior distribution. For the nucleon on a lattice with a  $\approx 310$  MeV pion mass and a box size of  $\approx 2.4$  fm, we prior the first three excited states in the following order: the Roper resonance ( $\approx 450$  MeV from the ground state), the two-pion excitation ( $\approx 180$  MeV from the Roper), and the  $L = 1$  one-pion excitation ( $\approx 110$  MeV from the two-pion excitation), with prior widths which accommodate a one-pion splitting (310 MeV) within  $1\sigma$ . For the fourth excited state onward, the prior for the energy splitting is set to the one-pion splitting while accommodating the two-pion splitting within  $1\sigma$ .

The excited state overlap factors can enter with an unknown sign (point-smeared), therefore as to not bias our expectation, we set the prior central values of the excited state overlap factors to zero. Due to smearing, we expect less overlap with excited states, and therefore set the width of  $\tilde{z}_n^S$  to half the value of the  $\tilde{z}_0^S$  central value. For the point-like overlap factor, we expect equal support from all states and therefore set the width of  $\tilde{z}_n^P$  to the value of the  $\tilde{z}_0^P$  central value.

#### 2. Discussion

We study the stability of  $\hat{E}_0$  from the two-point correlator fits under variation of the fit region and fit ansatz as shown in Figs. 6 and 7.

Perfect stability under varying number of states is demonstrated from fits in Fig. 6 with  $t_{\min} \geq 3$ , suggest-

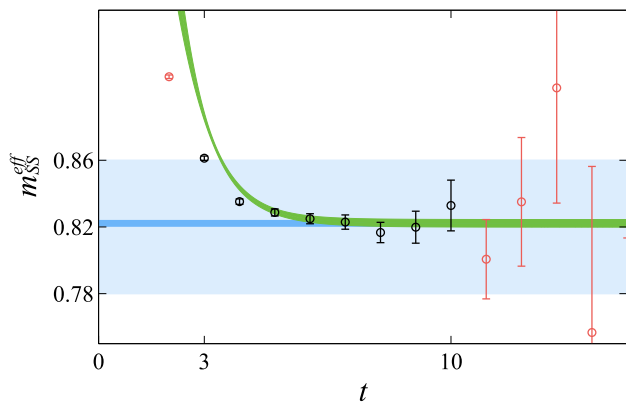


FIG. 2. Plot of the smeared-sink effective mass as a function of source-sink separation time  $t$ . The black points highlight the data used in the fit presented. The light blue bands indicate the  $1\sigma$  width of the ground state energy prior  $\tilde{E}_0$ , the dark blue bands show the central value and  $1\sigma$  uncertainty of the corresponding posterior distribution. The green bands are the resulting fit curves from a simultaneous fit to the smeared- and point-sink two-point correlation functions.

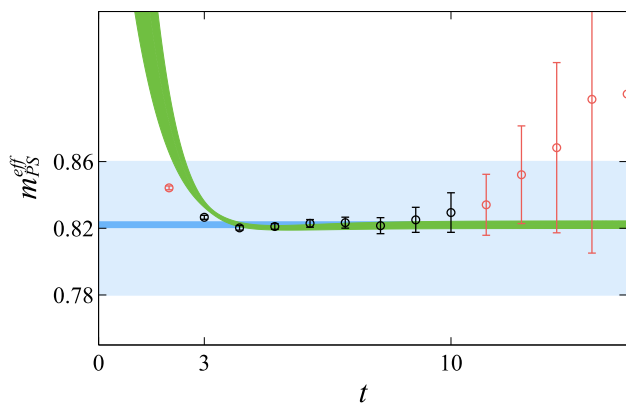


FIG. 3. Same as Fig. 2 but for the point-sink effective mass.

ing that we have controlled all the excited state systematic uncertainty. The fits show that more excited states are needed to achieve stability when including data with smaller  $t_{min}$  due to larger excited state contamination. We also observe that for all fit variations at a fixed  $t_{min}$  the Bayes Factor always prefers the stable fit result with the lowest number of excited states, as indicated by the solid symbols. We conclude that the increased uncertainty and variation of the central value from fits beyond  $t_{min} = 3$  are only due to omitting parts of the usable dataset. Therefore the preferred two-point fit is a 7 state fit with  $t = [3, 10]$ . We note that all fits with  $t_{min} = 2$  do not pass the  $Q$ -value criterion and are not considered. Similarly, Fig. 7 shows stability under varying  $t_{max}$  for the preferred fit and suggests that  $t_{max} = 10$  is adequate.

The preferred fit is plotted in Figs. 2–5 as a green band and agrees with the data in the selected fit region, which is indicated by the black data points. Inconsistency with

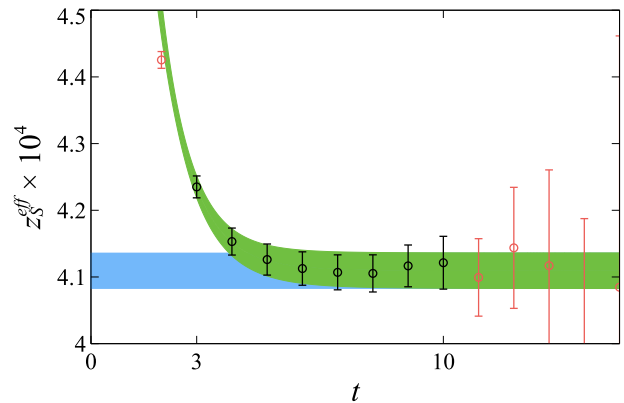


FIG. 4. Plot of the scaled two-point correlation function as a function of source-sink separation time  $t$  for the smeared overlap factor. The color scheme follows Fig. 2. The prior width exceeds the range of the y-axis, and is therefore not included in the plot.

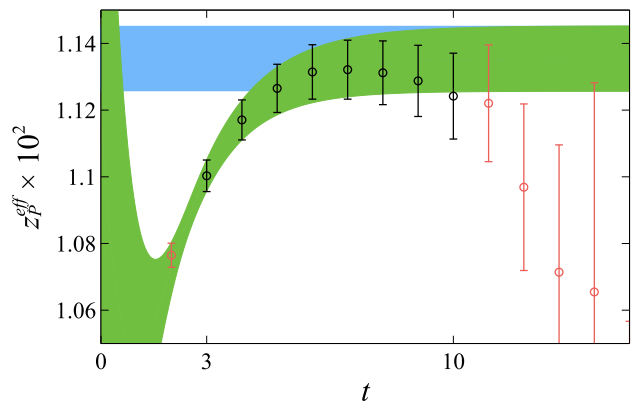


FIG. 5. Same as Fig. 4 but for the point-like overlap factor.

a few points (here at smaller  $t_{min}$ ) is expected for a fit with  $Q \approx 0.3$ . The ground state parameters  $E_0$ ,  $z_0^S$  and  $z_0^P$  are recovered in the  $t \rightarrow \infty$  limit from the effective mass and scaled correlators by construction. This is demonstrated by observing that the green fit band overlaps with the dark blue posterior band asymptotically at large  $t$ .

### C. Three-point correlator analysis

#### 1. Fit strategy

The three-point fit ansatz is given by Eq. (34). In addition to redefining the overlap factors  $z_n \equiv Z_n/\sqrt{2E_n}$ ,

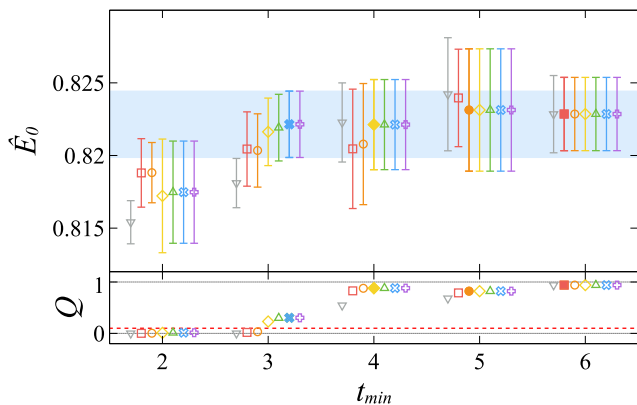


FIG. 6. Stability plots for the two-point correlation function. Stability plot under varying  $t_{min}$  with fixed  $t_{max} = 10$  is shown for fits with 2 states ( $\nabla$ ), 3 states ( $\blacksquare$ ), 4 states ( $\bullet$ ), 5 states ( $\blacklozenge$ ), 6 states ( $\blacktriangle$ ), 7 states ( $\blackstar$ ), and 8 states ( $\blackplus$ ). The corresponding  $Q$ -values of the fits are plotted below with the dashed line set at  $Q = 0.1$ . The solid symbols mark the fit with the largest Bayes factor at fixed  $t_{min}$ . The blue band highlights the preferred fit with 7 states at  $t_{min} = 3$  and guides the eye for observing stability.

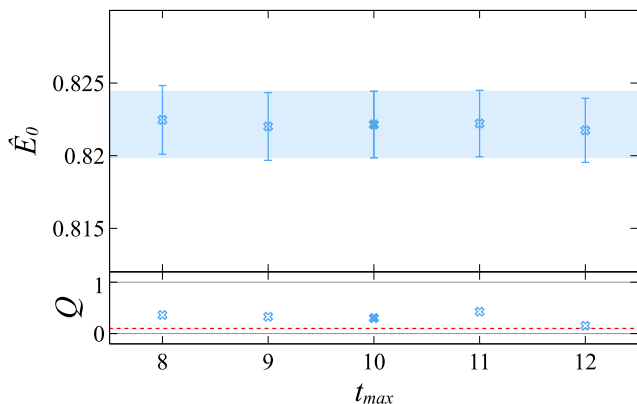


FIG. 7. Stability plot under varying  $t_{max}$  for the 7 state fit with  $t_{min} = 3$ . The color scheme follows Fig. 6. The solid symbol denotes the preferred two-point correlator fit.

we redefine the parameters with the following choices,

$$g_{nm} \equiv \frac{J_{nm}}{\sqrt{4E_n E_m}}, \quad (46)$$

$$d_n \equiv Z_n Z_{J:n}^\dagger + Z_{J:n} Z_n^\dagger + Z_n Z_n^\dagger \langle \Omega | J | \Omega \rangle + \sum_j \frac{Z_n Z_{nj}^\dagger J_j^\dagger + J_j Z_{jn} Z_n^\dagger}{2E_j (e^{E_j} - 1)}. \quad (47)$$

As a result, the three-point fit ansatz we employ throughout the rest of the analysis is,

$$N(t) = \sum_n [(t-1)z_n g_{nn} z_n^\dagger + d_n] e^{-E_n t} + \sum_{n \neq m} z_n g_{nm} z_m^\dagger \frac{e^{-E_n t} e^{\frac{\Delta_{nm}}{2}} - e^{-E_m t} e^{\frac{\Delta_{mn}}{2}}}{e^{\frac{\Delta_{nm}}{2}} - e^{\frac{\Delta_{mn}}{2}}}. \quad (48)$$

Under reparameterization, the three-point fit ansatz introduces additional parameters  $g_{nm}$  and  $d_n$  which are not constrained by the two-point correlator. In the following section, we detail how priors are chosen for the additional parameters, and study stability under variations of fit region and number of states.

We set the ground state prior  $\tilde{g}_{00}$  by constructing the derivative effective mass given by Eq. (14). By construction the derivative effective mass plateaus to  $g_{00}$  in the  $t \rightarrow \infty$  limit. Motivated by Figs. 8 and 9, we set  $\tilde{g}_{00} = 1.2(5)$  and observe that the prior widths are approximately one order of magnitude larger than the width of the posterior distributions.

The prior for  $d_0^{SS(PS)}$  is chosen by observing that

$$N^{SS(PS)}(1) = \sum_n d_n^{SS(PS)} e^{-E_n} \quad (49)$$

and assuming that the contribution to the infinite sum is primarily from the  $n = 0$  state due to operator smearing. This unique feature of the correlator at  $t = 1$  is exemplified in Figs. 10 and 11. Therefore we set the central value of  $\tilde{d}_0^{SS(PS)} = N^{SS(PS)}(1) e^{E_0} / 2$  with a prior width accommodating  $d_0^{SS(PS)} = 0$  within  $1\sigma$ .

For the excited state priors, we set  $\tilde{g}_{nm} = 0(1)$  to be the same order of magnitude as  $\tilde{g}_{00}$ . The overlap factor  $d_n^{SS(PS)}$  is set with a central value of  $\tilde{d}_n^{SS(PS)} = 0$  and with the same width as  $\tilde{d}_0^{SS(PS)}$ . This choice follows the same logic used to set the priors for  $z_n^S$ .

## 2. Discussion

The stability of  $\hat{g}_{00}$  under varying fit region and number of excited states is shown in Figs. 12 and 13. For all simultaneous two- and three-point fits, we perform the preferred two-point fit as discussed in Sec. III B.

For fits with  $t_{min} = 2, 3$ , Fig. 12 shows stability under varying the number of states for fits with more than 5 states, while the Bayes Factor prefers the 5 state fit (solid yellow diamonds). For fits with  $t_{min} \geq 4$ , we also observe stability, however the Bayes Factor prefers fits with less parameters ( $< 4$  states) over fits that qualitatively look more stable ( $\geq 5$  states), suggesting that there is not enough data to support fits with a large number of states. The fit at  $t_{min} = 1$  is stable after 7 states, however Eq. (49) shows that  $t = 1$  includes no information about  $g_{00}$ , the parameter of interest. Therefore for this



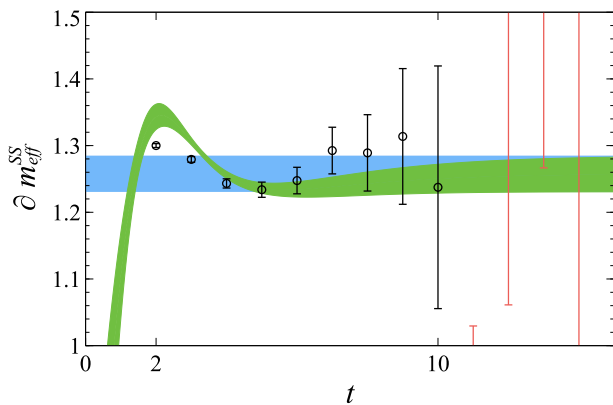


FIG. 8. Plot of the derivative effective mass as a function of source-sink separation time  $t$  for the smeared sink correlation functions. The color scheme follows Fig. 2. The prior width exceeds the range of the y-axis, and is therefore not included in the plot.

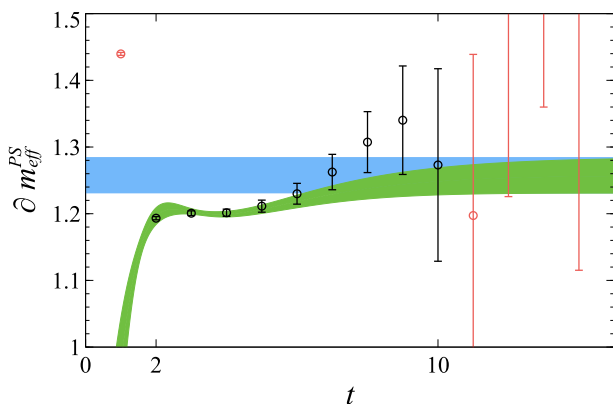


FIG. 9. Same as Fig. 8 for the point-sink correlation function.

study, we choose the 5 state fit with  $t = [2, 10]$  as the preferred fit. The preferred fit is shown to be insensitive under variations of  $t_{max}$  as demonstrated in Fig. 13.

The posterior distributions from the simultaneous fit are used to reconstruct the fitted curve and are shown by the green bands in Figs. 8 and 9. Similar to the effective mass and scaled correlator, we recover  $g_{00}$  in the  $t \rightarrow \infty$  limit, as shown by the exact overlap of  $\hat{g}_{00}$  and the green fit curve in the large  $t$  limit. Following this analysis we quote the value of the bare axial charge

$$\hat{g}_A = 1.258(27) \quad (50)$$

on the  $a \approx 0.15$  fm lattice with  $m_\pi \approx 310$  MeV. Determining the axial renormalization factor requires calculations at multiple quark masses to allow for an extrapolation to the chiral limit, which we do not perform in this work. These calculations used MDWF fermions, allowing for a determination of  $Z_A$  by computing the pion decay constant with both the conserved 5-d axial ward identity and with the non-conserved 4-d current. We find for this

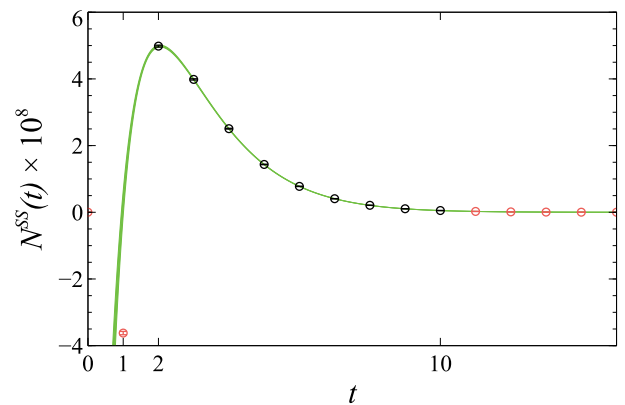


FIG. 10. Plot of the three-point correlator as a function of source-sink separation time  $t$  for the smeared-sink correlation functions. The color scheme follows Fig. 2. Note the distinct behavior of the  $N(t)$  correlation function at  $t = 1$  as discussed earlier.

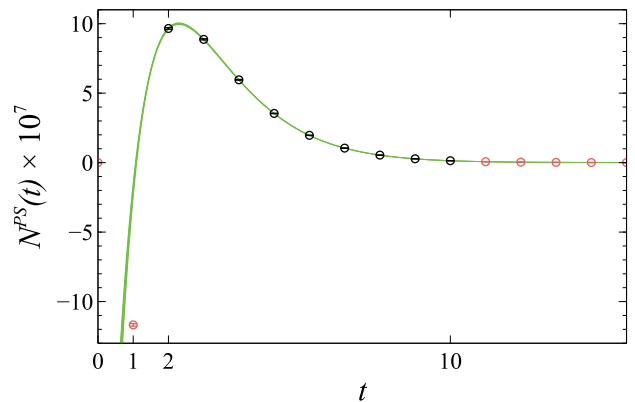


FIG. 11. Same as Fig. 10 for the point-sink  $N(t)$  function.

ensemble

$$Z_A = 0.9646(6). \quad (51)$$

While this is a quark-mass dependent renormalization, we can still compare our renormalized value of  $g_A$  with that determined using clover valence quarks on similar HISQ ensembles in Ref. [49]. They found  $g_A = 1.221(28)$  at  $m_\pi \approx 310$  MeV with  $a \approx 0.12$  fm, as compared to our value of

$$Z_A \hat{g}_A = 1.213(26). \quad (52)$$

#### IV. GENERALIZATIONS

The generalization of this method to non-zero momentum transfer and/or flavor changing currents is straightforward. To inject momentum with the current, instead of summing over a constant operator, the Feynman-Hellmann propagator would be constructed with a mo-

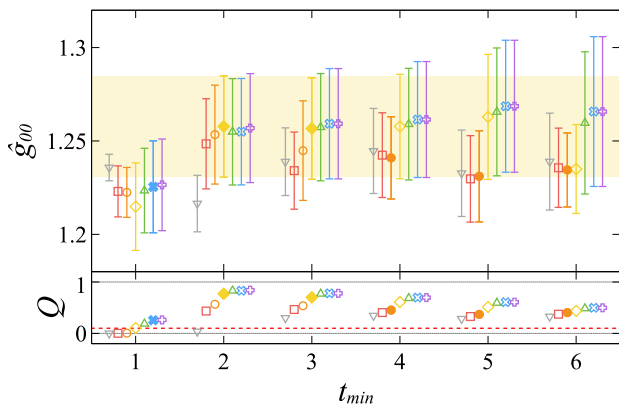


FIG. 12. Stability plots for the three-point correlation function. Stability plot under varying  $t_{min}$  with fixed  $t_{max} = 10$  is shown for fits with 2 to 8 states analogous to Fig. 6. The corresponding  $Q$ -values of the fits are plotted below the dashed line set at  $Q = 0.1$ . The solid symbols mark the fit with the largest Bayes factor at fixed  $t_{min}$ . The yellow band highlights the preferred fit with 5 states at  $t_{min} = 2$  and guides the eye for observing stability.

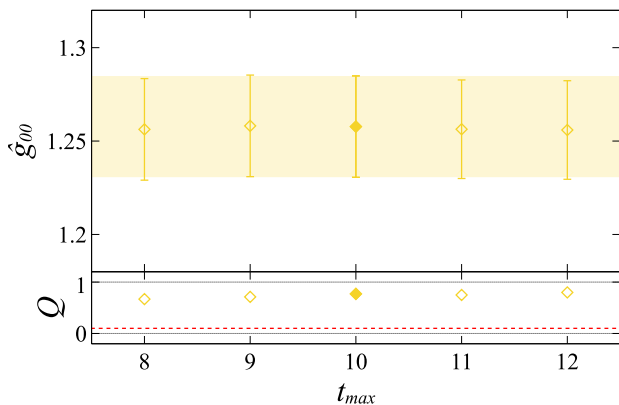


FIG. 13. Stability plot under varying  $t_{max}$  for the 7 state fit with  $t_{min} = 3$ . The solid symbol denotes the preferred two-point correlator fit.

mentum phase

$$S_q^\Gamma(y, x) = \sum_{z=(t_z, \mathbf{z})} e^{iq \cdot z} S(y, z) \Gamma S(z, x). \quad (53)$$

More complicated space-time dependent current insertions could also be considered. The modification of the numerator function is also straightforward. Unlike Eq. (22), the energy of the incoming and outgoing states would no longer be equal,  $E_m(p) \neq E_n(p+q)$  for any of the states  $|n\rangle$  and  $|m\rangle$ . The exception would be if the calculation is performed in the Breit Frame when  $\mathbf{p} + \mathbf{q} = -\mathbf{p}$ . In this case, the numerator expression from region I would still be given by Eq. (25). Else, the entire contribution from region I is parameterized by the second term in Eq. (25) where the state labels  $n$  and  $m$  now carry information about the momentum as well.

Flavor changing interactions are just as straightforward. In this case, the Feynman-Hellmann propagator is constructed as

$$S_{j \leftarrow i}^\Gamma(y, x) = \sum_{z=(t_z, \mathbf{z})} S_j(y, z) \Gamma S_i(z, x), \quad (54)$$

for a flavor changing interaction  $i \rightarrow j$ , with a trivial generalization to include momentum transfer as well. As with non-zero momentum transfer, the numerator expression from region I simplifies to just the second line of Eq. (25) as the energies of the incoming and outgoing states will not match.

This method can also be extended to consider two current insertions. A feasible technique for calculating two-current insertion matrix elements is needed to permit the LQCD evaluation of, *e.g.*, two-photon corrections to the Lamb shift in muonic helium-3 ions [50], which may shed light on the proton radius problem, and the  $\gamma$ - $Z$  box diagram corrections to electromagnetic structure functions [51] needed to improve the interpretation of results from the  $Q_{weak}$  experiment [52].

We first generalize Eqs. (3)–(5) to include multiple currents  $J_i$  with associated couplings  $\lambda_i$ . In the presence of multiple currents, the modified action of Eq. (4) is

$$S_\lambda = \lambda \cdot \int dt \mathbf{J}(t). \quad (55)$$

Two-current-insertion matrix elements can then be associated with the second derivative of the effective mass,

$$\left. \frac{\partial^2 m_\lambda^{eff}(t, \tau)}{\partial \lambda_i \partial \lambda_j} \right|_{\lambda=0} = \frac{1}{\tau} \left[ R_{ij}(t + \tau) - R_{ij}(t) - R_i(t + \tau) R_j(t + \tau) + R_i(t) R_j(t) \right]. \quad (56)$$

where  $R_i$  is a generalization of Eq. (15),

$$R_i(t) \equiv \frac{\int dt' \langle \Omega | T \{ \mathcal{O}(t) J_i(t') \mathcal{O}^\dagger(0) \} | \Omega \rangle}{C(t)}, \quad (57)$$

and  $R_{ij}$  is the ratio of the two-current insertion matrix element to the two-point function,

$$R_{ij}(t) \equiv \frac{\int dt' dt'' \langle \Omega | T \{ \mathcal{O}(t) J_i(t') J_j(t'') \mathcal{O}^\dagger(0) \} | \Omega \rangle}{C(t)}. \quad (58)$$

Like the first derivative of the effective mass in Eq. (14), the second derivative of the effective mass (*i.e.* Eq. (56)) benefits from an exact cancellation of the vacuum matrix elements of  $J_i$ ,  $J_j$ , and  $J_i J_j$ . The spectral decomposition of Eq. (56) precedes in analogy with that outlined in section II A, albeit with a few added complications that we intend to address in future work.

## V. CONCLUSIONS AND OUTLOOK

This work presents a computationally efficient and the most comprehensive implementation of lattice calculations of hadronic matrix elements utilizing the Feynman-Hellmann Theorem. The efficiency is achieved by first

analytically evaluating the derivative with respect to the source of an external current prior to performing any lattice calculations. Derivation of systematic effects associated with this method, including excited state contamination, mesonic propagating modes, and signal from contact operators are completely presented up to terms suppressed by  $\mathcal{O}(e^{-E_n T})$ , where corrections to include higher order thermal effect are self-evident.

The example calculation of the nucleon axial charge demonstrates that from the calculation of a low-statistics run, we are able to achieve a 2.1% uncertainty on  $g_A$ , all systematic errors from the fitting procedure inclusive. The benefits of increased stochastic sampling is made possibly by 1) the sum over the current insertion time  $t'$  leading to  $\mathcal{O}(T)$  increase in statistics and 2) the ability to explore fits with multiple source-sink separations, allowing for the eventual *exponential* gain in the signal-over-noise ratio due to fitting to a source-sink separation of  $\approx 0.45$  fm ( $t_{min} = 3$ ). Access to all source-sink separations also allows us to demonstrate complete control over all systematic uncertainties originating from the fitting procedure.

The generalization of this method to non-zero momentum transfer, flavor changing currents, and multiple current insertions is straightforward. The ideas presented here are not restricted to lattice field theory calculations, but applicable to any theory with the notion of a bi-linear current.

## ACKNOWLEDGMENTS

The LQCD calculations for this work utilized a modification of the Chroma software suite [53], the *irresponsibly* fast QUDA library [40, 41] and the highly efficient HDF5 I/O Library [54] with an interface to HDF5 in the USQCD Software Stack added with CalLat SciDAC 3 support [55]. The calculations were performed at the Jefferson Lab High Performance Computing Center on facilities of the USQCD Collaboration, which are funded by the Office of Science of the U.S. Department of Energy, and at LLNL through a Multiprogrammatic and Institutional Computing program for the Grand Challenge allocation.

This research was supported in part by The U.S. Department of Energy, Office of Science; under contract number DE-AC05-06OR23177, which Jefferson Science Associates, LLC, manages and operates the Jefferson Lab (KNO, AWL); under contract number DE-AC02-05CH11231, which the Regents of the University of California manage and operate Lawrence Berkeley National Laboratory and the National Energy Research Scientific Computing Center (CCC, TK, AWL); Office of Nuclear Physics under Grant Number DE-FG02-04ER41302 (CMB, KNO), and the Double-Beta Decay Topical Collaboration under Contract number DE-SC0015376 (AWL); Office of Advanced Scientific Computing Research, Scientific Discovery through Advanced Computing (SciDAC) program under Award Number KB0301052 (TK, AWL); The Office of Nuclear Physics The DOE Early Career Research Program, Office of Nuclear Physics under FWP Number NQCDAWL (CCC, AWL).

- 
- [1] Güttinger, P., *Zeitschrift für Physik* **73**, 169 (1932).  
 [2] W. Pauli, *Principles of Wave Mechanics*, Vol. 24 (Springer, 1933) p. 162.  
 [3] H. Hellmann, *Einführung in die Quantenchemie* (Franz Deuticke, 1937) p. 285, OL21481721M.  
 [4] R. P. Feynman, *Phys. Rev.* **56**, 340 (1939).  
 [5] M. Procura, T. R. Hemmert, and W. Weise, *Phys. Rev.* **D69**, 034505 (2004), arXiv:hep-lat/0309020 [hep-lat].  
 [6] M. Procura, B. U. Musch, T. Wollenweber, T. R. Hemmert, and W. Weise, *Phys. Rev.* **D73**, 114510 (2006), arXiv:hep-lat/0603001 [hep-lat].  
 [7] C. Alexandrou *et al.* (European Twisted Mass), *Phys. Rev.* **D78**, 014509 (2008), arXiv:0803.3190 [hep-lat].  
 [8] A. Walker-Loud, H.-W. Lin, D. Richards, R. Edwards, M. Engelhardt, *et al.*, *Phys. Rev.* **D79**, 054502 (2009), arXiv:0806.4549 [hep-lat].  
 [9] H. Ohki, H. Fukaya, S. Hashimoto, T. Kaneko, H. Matsufuru, J. Noaki, T. Onogi, E. Shintani, and N. Yamada, *Phys. Rev.* **D78**, 054502 (2008), arXiv:0806.4744 [hep-lat].  
 [10] R. D. Young and A. W. Thomas, *Phys. Rev.* **D81**, 014503 (2010), arXiv:0901.3310 [hep-lat].  
 [11] S. Durr *et al.*, *Phys. Rev.* **D85**, 014509 (2012), [Erratum: *Phys. Rev.* **D93**, no.3, 039905 (2016)], arXiv:1109.4265 [hep-lat].  
 [12] R. Horsley, Y. Nakamura, H. Perlt, D. Pleiter, P. E. L. Rakow, G. Schierholz, A. Schiller, H. Stuben, F. Winter, and J. M. Zanotti (QCDSF-UKQCD), *Phys. Rev.* **D85**, 034506 (2012), arXiv:1110.4971 [hep-lat].  
 [13] W. Freeman and D. Toussaint (MILC), *Phys. Rev.* **D88**, 054503 (2013), arXiv:1204.3866 [hep-lat].  
 [14] G. S. Bali *et al.*, *Nucl. Phys.* **B866**, 1 (2013), arXiv:1206.7034 [hep-lat].  
 [15] H. Ohki, K. Takeda, S. Aoki, S. Hashimoto, T. Kaneko, H. Matsufuru, J. Noaki, and T. Onogi (JLQCD), *Phys. Rev.* **D87**, 034509 (2013), arXiv:1208.4185 [hep-lat].  
 [16] A. Semke and M. F. M. Lutz, *Phys. Lett.* **B717**, 242 (2012), arXiv:1202.3556 [hep-ph].  
 [17] P. E. Shanahan, A. W. Thomas, and R. D. Young, *Phys. Rev.* **D87**, 074503 (2013), arXiv:1205.5365 [nucl-th].  
 [18] X. L. Ren, L. S. Geng, J. Martin Camalich, J. Meng, and H. Toki, *JHEP* **12**, 073 (2012), arXiv:1209.3641 [nucl-th].  
 [19] P. Junnarkar and A. Walker-Loud, *Phys. Rev.* **D87**, 114510 (2013), arXiv:1301.1114 [hep-lat].  
 [20] S. Durr *et al.*, *Phys. Rev. Lett.* **116**, 172001 (2016), arXiv:1510.08013 [hep-lat].

- [21] R. J. Hill and M. P. Solon, *Phys. Rev. Lett.* **112**, 211602 (2014), [arXiv:1309.4092 \[hep-ph\]](#).
- [22] A. Chambers *et al.* (CSSM, QCDSF/UKQCD), *Phys.Rev.* **D90**, 014510 (2014), [arXiv:1405.3019 \[hep-lat\]](#).
- [23] A. J. Chambers *et al.*, *Phys. Rev.* **D92**, 114517 (2015), [arXiv:1508.06856 \[hep-lat\]](#).
- [24] F. Fucito, G. Parisi, and S. Petrarca, *Phys. Lett.* **B115**, 148 (1982).
- [25] G. Martinelli, G. Parisi, R. Petronzio, and F. Rapuano, *Phys. Lett.* **B116**, 434 (1982).
- [26] C. W. Bernard, T. Draper, K. Olynyk, and M. Rushton, *Phys. Rev. Lett.* **49**, 1076 (1982).
- [27] W. Detmold, B. Tiburzi, and A. Walker-Loud, *Phys.Rev.* **D73**, 114505 (2006), [arXiv:hep-lat/0603026 \[hep-lat\]](#).
- [28] M. Engelhardt (LHPC), *Phys. Rev.* **D76**, 114502 (2007), [arXiv:0706.3919 \[hep-lat\]](#).
- [29] W. Detmold, B. C. Tiburzi, and A. Walker-Loud, *Phys. Rev.* **D79**, 094505 (2009), [arXiv:0904.1586 \[hep-lat\]](#).
- [30] W. Detmold, B. Tiburzi, and A. Walker-Loud, *Phys.Rev.* **D81**, 054502 (2010), [arXiv:1001.1131 \[hep-lat\]](#).
- [31] M. J. Savage, P. E. Shanahan, B. C. Tiburzi, M. L. Wagman, F. Winter, S. R. Beane, E. Chang, Z. Davoudi, W. Detmold, and K. Orginos, (2016), [arXiv:1610.04545 \[hep-lat\]](#).
- [32] S. Basak, R. G. Edwards, G. T. Fleming, U. M. Heller, C. Morningstar, D. Richards, I. Sato, and S. Wallace, *Phys. Rev.* **D72**, 094506 (2005), [arXiv:hep-lat/0506029 \[hep-lat\]](#).
- [33] S. Basak, R. Edwards, G. T. Fleming, U. M. Heller, C. Morningstar, D. Richards, I. Sato, and S. J. Wallace (Lattice Hadron Physics (LHPC)), *Phys. Rev.* **D72**, 074501 (2005), [arXiv:hep-lat/0508018 \[hep-lat\]](#).
- [34] L. Maiani, G. Martinelli, M. L. Paciello, and B. Taglienti, *Nucl. Phys.* **B293**, 420 (1987).
- [35] G. M. de Divitiis, R. Petronzio, and N. Tantalo, *Phys. Lett.* **B718**, 589 (2012), [arXiv:1208.5914 \[hep-lat\]](#).
- [36] C. Alexandrou, S. Dinter, V. Drach, K. Jansen, K. Hadjiyiannakou, and D. B. Renner (ETM), *Eur. Phys. J.* **C74**, 2692 (2014), [arXiv:1302.2608 \[hep-lat\]](#).
- [37] E. Follana, Q. Mason, C. Davies, K. Hornbostel, G. P. Lepage, J. Shigemitsu, H. Trotter, and K. Wong (HPQCD, UKQCD), *Phys. Rev.* **D75**, 054502 (2007), [arXiv:hep-lat/0610092 \[hep-lat\]](#).
- [38] A. Bazavov *et al.* (MILC), *Phys. Rev.* **D87**, 054505 (2013), [arXiv:1212.4768 \[hep-lat\]](#).
- [39] R. C. Brower, H. Neff, and K. Orginos, (2012), [arXiv:1206.5214 \[hep-lat\]](#).
- [40] M. Clark, R. Babich, K. Barros, R. Brower, and C. Rebbi, *Comput.Phys.Commun.* **181**, 1517 (2010), [arXiv:0911.3191 \[hep-lat\]](#).
- [41] R. Babich, M. Clark, B. Joo, G. Shi, R. Brower, *et al.*, (2011), [arXiv:1109.2935 \[hep-lat\]](#).
- [42] E. Berkowitz, C. Bouchard, C. Chang, K. Clark, B. Joo, T. Kurth, K. McElvain, C. Monahan, A. Nicholson, K. Orginos, E. Rinaldi, P. Vranas, and A. Walker-Loud, “Möbius Domain-Wall fermions on gradient-flowed HISQ configurations,” *in preparation*.
- [43] A. Nicholson, E. Berkowitz, C. C. Chang, M. A. Clark, B. Joo, T. Kurth, E. Rinaldi, B. Tiburzi, P. Vranas, and A. Walker-Loud, in *Proceedings, 34th International Symposium on Lattice Field Theory (Lattice 2016): Southampton, UK, July 24-30, 2016* (2016) [arXiv:1608.04793 \[hep-lat\]](#).
- [44] G. P. Lepage, B. Clark, C. T. H. Davies, K. Hornbostel, P. B. Mackenzie, C. Morningstar, and H. Trotter, *Contents of lattice 2001 proceedings*, *Nucl. Phys. Proc. Suppl.* **106**, 12 (2002), [12(2001)], [arXiv:hep-lat/0110175 \[hep-lat\]](#).
- [45] Y. Chen, S.-J. Dong, T. Draper, I. Horvath, K.-F. Liu, N. Mathur, S. Tamhankar, C. Srinivasan, F. X. Lee, and J.-b. Zhang, (2004), [arXiv:hep-lat/0405001 \[hep-lat\]](#).
- [46] B. Yoon *et al.*, (2016), [arXiv:1611.07452 \[hep-lat\]](#).
- [47] A. Bazavov *et al.* (Fermilab Lattice, MILC), *Phys. Rev.* **D93**, 113016 (2016), [arXiv:1602.03560 \[hep-lat\]](#).
- [48] G. P. Lepage, “**lsqfit v8.1**,” (2016).
- [49] T. Bhattacharya, V. Cirigliano, S. Cohen, R. Gupta, H.-W. Lin, and B. Yoon, *Phys. Rev.* **D94**, 054508 (2016), [arXiv:1606.07049 \[hep-lat\]](#).
- [50] C. E. Carlson, M. Gorchtein, and M. Vanderhaeghen, ([arXiv:1611.06192](#)), [arXiv:1611.06192 \[nucl-th\]](#).
- [51] B. C. Rislow and C. E. Carlson, *Phys. Rev.* **D88**, 013018 (2013), [arXiv:1304.8113 \[hep-ph\]](#).
- [52] D. Andreic, D. S. Armstrong, A. Asaturyan, T. Averett, J. Balewski, J. Beaufait, R. S. Beminiwattha, J. Benesch, F. Benmokhtar, J. Birchall, R. D. Carlini, G. D. Cates, J. C. Cornejo, S. Covrig, M. M. Dalton, C. A. Davis, W. Deconinck, J. Diefenbach, J. F. Dowd, J. A. Dunne, D. Dutta, W. S. Duvall, M. Elaasar, W. R. Falk, J. M. Finn, T. Forest, D. Gaskell, M. T. W. Gericke, J. Grames, V. M. Gray, K. Grimm, F. Guo, J. R. Hoskins, K. Johnston, D. Jones, M. Jones, R. Jones, M. Kargiantoulakis, P. M. King, E. Korkmaz, S. Kowalski, J. Leacock, J. Leckey, A. R. Lee, J. H. Lee, L. Lee, S. MacEwan, D. Mack, J. A. Magee, R. Mahurin, J. Mammei, J. W. Martin, M. J. McHugh, D. Meekins, J. Mei, R. Michaels, A. Micherdzinska, A. Mkrtchyan, H. Mkrtchyan, N. Morgan, K. E. Myers, A. Narayan, L. Z. Ndukum, V. Nelyubin, Nuruzzaman, W. T. H. van Oers, A. K. Oppen, S. A. Page, J. Pan, K. D. Paschke, S. K. Phillips, M. L. Pitt, M. Poelker, J. F. Rajotte, W. D. Ramsay, J. Roche, B. Sawatzky, T. Seva, M. H. Shabestari, R. Silwal, N. Simicevic, G. R. Smith, P. Solvignon, D. T. Spayde, A. Subedi, R. Subedi, R. Suleiman, V. Tadevosyan, W. A. Tobias, V. Tvaskis, B. Waidyawansa, P. Wang, S. P. Wells, S. A. Wood, S. Yang, R. D. Young, and S. Zhamkochyan (*Q<sub>weak</sub>* Collaboration), *Phys. Rev. Lett.* **111**, 141803 (2013).
- [53] R. G. Edwards and B. Joo (SciDAC Collaboration, LHPC Collaboration, UKQCD Collaboration), *Nucl.Phys.Proc.Suppl.* **140**, 832 (2005), [arXiv:hep-lat/0409003 \[hep-lat\]](#).
- [54] The HDF Group, “Hierarchical Data Format, version 5,” (1997-NNNN), <http://www.hdfgroup.org/HDF5/>.
- [55] T. Kurth, A. Pochinsky, A. Sarje, S. Syritsyn, and A. Walker-Loud, *Proceedings, 32nd International Symposium on Lattice Field Theory (Lattice 2014): Brookhaven, NY, USA, June 23-28, 2014*, PoS **LAT-TICE2014**, 045 (2015), [arXiv:1501.06992 \[hep-lat\]](#).